

Structure and Electronic Configurations of the Intermediates of Water Oxidation in Blue Ruthenium Dimer Catalysis

Dooshaye Moonshiram,[†] Jonah W. Jurs,^{‡,§} Javier J. Concepcion,[‡] Taisiya Zakharova,[†] Igor Alperovich,^{†,§} Thomas J. Meyer,[‡] and Yulia Pushkar^{*†}

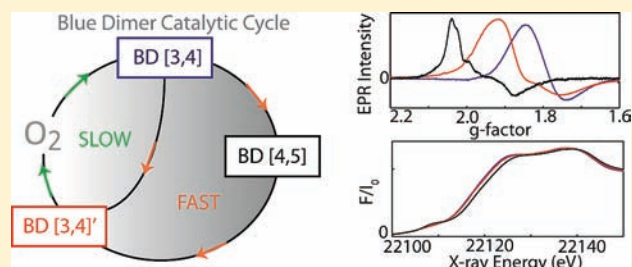
[†]Department of Physics, Purdue University, 525 Northwestern Avenue West Lafayette, Indiana 47907, United States

[‡]Department of Chemistry, University of North Carolina at Chapel Hill, Chapel Hill, North Carolina 27599, United States

[§]Research Center for Nanoscale Structure of Matter, Southern Federal University, 5 Zorge Street, 344090, Rostov-on-Don, Russian Federation

Supporting Information

ABSTRACT: Catalytic O₂ evolution with *cis,cis*-[(bpy)₂(H₂O)-Ru^{III}ORu^{III}(OH₂)(bpy)₂]⁴⁺ (bpy is 2,2-bipyridine), the so-called blue dimer, the first designed water oxidation catalyst, was monitored by UV–vis, EPR, and X-ray absorption spectroscopy (XAS) with ms time resolution. Two processes were identified, one of which occurs on a time scale of 100 ms to a few seconds and results in oxidation of the catalyst with the formation of an intermediate, here termed [3,4]'. A slower process occurring on the time scale of minutes results in the decay of this intermediate and O₂ evolution. Spectroscopic data suggest that within the fast process there is a short-lived transient intermediate, which is a precursor of [3,4]'. When excess oxidant was used, a highly oxidized form of the blue dimer [4,5] was spectroscopically resolved within the time frame of the fast process. Its structure and electronic state were confirmed by EPR and XAS. As reported earlier, the [3,4]' intermediate likely results from reaction of [4,5] with water. While it is generated under strongly oxidizing conditions, it does not display oxidation of the Ru centers past [3,4] according to EPR and XAS. EXAFS analysis demonstrates a considerably modified ligand environment in [3,4]'. Raman measurements confirmed the presence of the O–O fragment by detecting a new vibration band in [3,4]' that undergoes a 46 cm⁻¹ shift to lower energy upon ¹⁶O/¹⁸O exchange. Under the conditions of the experiment at pH 1, the [3,4]' intermediate is the catalytic steady state form of the blue dimer catalyst, suggesting that its oxidation is the rate-limiting step.



1. INTRODUCTION

Utilization of sunlight in energy applications requires light harvesting, energy conversion, and storage. One effective way to store energy is to convert it into chemical energy by fuel-forming reactions, such as water splitting into hydrogen and oxygen ($2\text{H}_2\text{O} + 4h\nu \rightarrow \text{O}_2 + 2\text{H}_2$) or water reduction of CO₂ to methanol ($2\text{H}_2\text{O} + \text{CO}_2 + 6h\nu \rightarrow \text{CH}_3\text{OH} + \frac{3}{2}\text{O}_2$), other oxygenates, or hydrocarbons. In photosynthesis, photosystem II (PSII) is a natural catalyst that captures sunlight and couples its energy to drive water splitting with high efficiency (>60%).¹

Direct conversion of light to chemical fuels by a synthetic device made of inorganic, organic, or hybrid materials is an attractive method for harvesting solar energy^{2–4} but one that requires efficient, robust, and economically feasible catalysts. In the absence of a serendipitous discovery, mechanistic knowledge is required for the design of such catalysts. Mechanistic insights can be acquired by spectroscopic analysis of short-lived intermediates of catalytic water oxidation. Use of techniques sensitive to the electronic states of molecules such as EPR and X-ray absorption spectroscopy (XAS) is thereby crucial to determine the electronic requirements for catalytic water oxidation.

A variety of heterogeneous water oxidation catalysts have been identified including the metal oxides of Ru,^{5,6} Ir,⁷ Mn, and Co, whose activities can be enhanced in nanoparticle preparations,^{8a} and a mixed Co-phosphate^{8b} oxide. Though promising for practical applications due to their economic feasibility, the 3d transition metal oxides studied are still less active than the PS II Mn₄Ca cluster. The surface complexity of heterogeneous water oxidation catalysts and protein complexity of PS II make elucidation of their catalytic mechanisms difficult.

Study of homogeneous catalysts offers promise in providing valuable insights about the mechanism of the water oxidation reaction. Ruthenium-based molecular water oxidation catalysts have been known since the early 1980s.^{10,11} Recently, a variety of stable ligands that can accommodate two Ru atoms have been developed, resulting in several catalytically active complexes.^{9,12–16} To improve the stability of such complexes, it has been proposed that organic ligands be replaced with an “all-inorganic” environment as in POM (polyoxometalate) frameworks.^{17–19} “Single-site” catalysts based on iridium and

Received: September 13, 2011

Published: February 14, 2012

ruthenium have also been identified and mechanism of their activity has been elucidated.^{20–24}

The blue dimer catalyst *cis,cis*-[(bpy)₂(H₂O)-Ru^{III}ORu^{III}(OH₂)(bpy)₂]⁴⁺ (bpy is 2,2-bipyridine) was chosen for this spectroscopic study as the most analyzed homogeneous system for catalytic water oxidation.^{9,12,25} For convenience in discussing the blue dimer, we will use square brackets to abbreviate the oxidation states of its Ru centers with [3,3] as the abbreviation for the parent complex. The large body of previous work on the blue dimer has resulted in the formulation of a paradigm for water oxidation with oxidative activation by proton coupled electron transfer (PCET) to intermediates containing Ru^V=O a key feature.^{10,11,25–29} Once formed, Ru^V=O species are proposed to be catalytically active toward oxygen–oxygen bond formation by reaction with water molecules to produce peroxidic intermediates. While the mechanism of water oxidation initiated by the blue dimer [5,5] was studied computationally,³⁰ the lack of experimental structural information on such species presents a considerable hurdle for evaluation of the proposed mechanism. Only one XAS structural study has been reported for highly oxidized blue dimer intermediates, presumably blue dimer [5,5] without thorough characterization of the chemical composition and purity of the sample.³¹ The proposed peroxo intermediate resulting from the reaction of Ru^V=O with water has never been structurally characterized. Blue dimer [5,5] can be formed with excess chemical oxidant or through electrolysis under highly oxidized potentials³² but its formation has not yet been demonstrated under conditions corresponding to a single catalytic turnover. A critical issue with the blue dimer catalyst is that at least three highly oxidized species [4,4], [4,5], and [5,5] can be formed and they all, from a thermodynamic standpoint, can oxidize water. Evaluation of their involvement as catalytic species is complicated by their overlapping UV–vis absorption spectra, which are also dependent on pH, and coordination of anions.¹²

In this study we chose to work at pH 1 to minimize the effects of the known acid–base equilibria of the blue dimer based on coordinated water: Ru–OH₂ⁿ⁺ = Ru–OH^{(n–1)+} + H⁺. Under these conditions, the Ru–OH₂ and Ru–OH groups in [5,5] and [4,5] are deprotonated based on pH-dependent electrochemical measurements.¹⁰ Blue dimer [4,4] is a short-lived, unstable intermediate under all conditions and its protonation state is unknown.^{26–33} Using the stable blue dimer [3,4] complex³ as starting material and ceric ammonium nitrate (hereafter denoted Ce(IV)) as a chemical oxidant we monitored the catalyst oxidation with UV–vis stopped-flow measurements. This allowed us to define time frames for collecting samples enriched with the short-lived intermediates by the freeze quench approach. Use of blue dimer [3,4] enabled us to avoid interference from the relatively slow kinetics associated with oxidation of [3,3] to [3,4] and utilization of Ce(IV) allowed us to initiate single-turnover conditions impossible to achieve with electrochemical oxidation of the catalyst.³⁴ The samples were characterized by EPR, Ru K-edge X-ray absorption near edge structure (XANES), and extended X-ray absorption fine structure (EXAFS). These techniques allowed us to assign the oxidation states of the Ru centers and determine the structural characteristics of the reactive intermediates. Parallel O₂ evolution measurements were used to confirm the presence of the detected intermediates under conditions of active O₂ evolution.

2. MATERIALS AND METHODS

2.1. Sample Preparations. Throughout this study the blue dimer was used as the PF₆[–] and ClO₄[–] salts and no differences between the two were observed. [((bpy)₂Ru^{III}(H₂O))₂O](PF₆)₄ was prepared from [((bpy)₂Ru^{III}(H₂O))₂O](ClO₄)₄, as previously described,¹¹ via salt metathesis by adding NH₄PF₆ to an aqueous solution of the ClO₄[–] salt. The blue dimer cation was purified by chromatography on LH-20 Sephadex. Blue dimer [3,4] was prepared by oxidation with 1 equiv of ceric ammonium nitrate, Ce^{IV}(NH₄)₂(NO₃)₆·4H₂O. It was used as it is or after additional purification and recrystallization with no differences noticed. Purity of blue dimer [3,3] and [3,4] was verified by comparison with known electrochemical and electronic spectra.¹¹ Ultrapure (Type 1) water (resistivity 18.2 MΩ·cm at 25 °C, TOC 4 μg/L) sourced from a Q-POD unit of a Milli-Q integral water purification system (Millipore) was used for solutions. All samples were prepared in 0.1 M HNO₃ acid, pH 1.0 (Catalog No. 225711 from Sigma Aldrich). Some titration experiments were conducted in 0.1 M CF₃SO₃H (freshly distilled) and samples were analyzed by EPR. No differences in EPR spectra were observed when 0.1 M HNO₃ or 0.1 M CF₃SO₃H acids were used as reaction media. Oxidant solutions were prepared fresh daily by dissolving Ce(NH₄)₂(NO₃)₆·4H₂O in 0.1 M HNO₃.

The Ru^V=O reference, tetra-*n*-propylammonium bis-2-hydroxy-2-ethylbutyrate(oxo) ruthenate (V), was prepared as described by Williams and co-workers.³⁵ Its EPR spectrum was recorded at 20 K and found to be identical with the spectrum of the original report.³⁵ The XANES of Ru^{IV} reference compound, ruthenium(IV) oxide, was measured to compare with that of blue dimer [3,3] and [3,4].

For isotopic exchange BD[3,3] was dissolved in 98% enriched ¹⁸O water (Icon Isotopes) and left for 24 h. BD [3,4] and [3,4]’ were subsequently prepared by adding Ce(IV).

2.2. UV–Vis, Stopped-Flow, Freeze-Quench. A Cary 300 Bio UV–vis spectrophotometer (Varian Inc.) was used to monitor UV–visible spectra of stable forms of the blue dimer [3,3] (637 nm—absorption maxima in 0.1 M HNO₃) and [3,4] (494 nm—absorption maxima in 0.1 M HNO₃) as well as changes in the absorbance versus time following oxidation. Analysis was conducted with concentrations of blue dimer in the range 0.5 × 10^{–4} to 2.5 × 10^{–4} M. A SX20 stopped-flow UV–vis spectrometer (Applied Photophysics Ltd.) with a dead time of 0.5 ms was used to follow the reactions. Changes in the absorbance were monitored from times as early as 1 ms after Ce(IV) addition. Cuvettes with path lengths of 2 and 10 mm were utilized to study changes in the absorbance of concentrated 0.25 × 10^{–3} to 0.1 × 10^{–3} M and less concentrated samples of 0.5 × 10^{–4} to 1 × 10^{–4} M, respectively. No principal differences were observed when blue dimer was oxidized in 10^{–4} M versus 10^{–5} M concentration ranges. Increases in the blue dimer concentration only resulted in increases in reaction rates as expected by rate law.

UV–visible absorption measurements were conducted in parallel with other spectroscopic techniques, namely EPR and XAS. To measure samples with EPR and XAS, fast freeze-quenching of reaction mixtures was performed by using an SFM 20 stopped-flow system (Bio-Logic Science Instruments). The apparatus is equipped with an umbilical connector with a built-in ejection nozzle at the end of the aging loop that sprays the aged reaction mixtures into precooled liquid pentane at –120 °C. This setup allows for freezing of reaction mixtures starting 1 ms after reagent mixing. **Warning:** Liquid pentane is flammable. Great care should be taken when storing and handling. Samples were collected from liquid pentane with EPR and XAS collection kits. Oxidized intermediates were prepared from blue dimer [3,4] by oxidation with Ce(IV) to form the intermediates reported in this study, namely blue dimer [4,5] and [3,4]’. To ensure that intermediates do not react with pentane at –120 °C, samples were also collected by spraying reaction mixtures into liquid nitrogen. Both the [3,4]’ and [4,5] intermediates were observed using pentane (–120 °C) as well as liquid nitrogen as cryogens. Liquid nitrogen provides a slower freezing rate and should not be used for monitoring short (less than 2 s) reactions.

2.3. Oxygen (O₂) Evolution Measurements. Oxygen evolution was measured with a PC operated Clark-type polarographic oxygen electrode from Oxygraph System (Hansatech Instruments Ltd.). The sample was housed within a hermetic borosilicate glass reaction vessel thus preventing penetration of any atmospheric oxygen. Calibration was carried out by measurements of the signal from O₂-saturated water in an open reaction vessel. Sodium dithionite, an oxygen-depleting agent, was added to the water and the drop in the signal was related to the solubility of oxygen in water at room temperature (262 μmol/L). The glass vessel was thoroughly washed with water and 1 mL of 0.1 mM blue dimer [3,3] was added. A defined number of equivalents of Ce(IV) was carefully added by means of a Hamilton syringe into the chamber through a septum cap and oxygen evolution was measured as a function of time.

2.4. EPR Measurements. Low-temperature X-band EPR spectra were recorded with a Bruker EMX X-band spectrometer equipped with a X-Band CW microwave bridge. The sample temperature was maintained at 20 K, unless otherwise indicated, by use of an Air Products LTR liquid helium cryostat. Spectrometer conditions were as follows: microwave frequency, 9.65 GHz; field modulation amplitude, 10 G at 100 kHz; microwave power, 31.70 mW. Standard EPR sample tubes were filled with sample through all of the resonator space and whenever relative signal intensities are discussed, measurements were conducted on the same day in the same conditions to allow direct comparison of the signal intensities. Field calibration was checked versus DPPH standard. Quantification of the EPR detectable species is given in Table S3 in the SI.

2.5. XAS and EXAFS Measurements. X-ray absorption spectra were collected at the Advanced Photon Source (APS) at Argonne National Laboratory on bending magnet beamline 20 at an electron energy of 23 keV and average current 100 mA. The radiation was monochromatized by a Si(110) crystal monochromator. The intensity of the X-rays was monitored by three ion chambers (I₀, I₁, and I₂) filled with 70% nitrogen and 30% argon and placed before the sample (I₀) and after the sample (I₁ and I₂). Ru metal was placed between the I₁ and I₂ and its absorption was recorded with each scan for energy calibration. Plastic (Lexan) EXAFS sample holders (inner dimensions of 12 mm × 3 mm × 3 mm) filled with frozen solutions or freeze-quenched samples were inserted into the precooled (20 K) cryostat. The samples were kept at 20 K in a He atmosphere at ambient pressure. Data were recorded as fluorescence excitation spectra, using a 13-element energy-resolving detector. Solid samples were diluted with BN powder in a 1:5 ratio, pressed between mylar tape, and measured in the cryostat in transmission mode. To reduce the risk of sample damage by X-ray radiation, 80% flux was used in the defocused mode (beam size 1 × 10 mm) and no damage was observed scan after scan to any samples. The samples were also protected from the X-ray beam during spectrometer movements by a shutter synchronized with the scan program. Additionally, low flux measurements (only 10% of beamline flux) were done on reactive intermediates to demonstrate the same EXAFS results. No more than 5 scans were taken at each sample position at any condition.

Ru XAS energy was calibrated by the first maxima in the second derivative of the ruthenium metal XANES spectrum (22117 eV). EXAFS data were collected during a total of five beamtimes. EXAFS scan with 10-eV steps in the pre-edge region (21967–22102 eV), 1-eV steps (22102–22117 eV) through the edge, and 0.05-Å⁻¹ steps from $k = 2.0$ to 16 Å⁻¹ were used. As reference compounds for high Ru oxidation states, Ru(IV) and Ru(V), Ru(IV) oxide, and tetra-n-propylammonium bis-2-hydroxy-2-ethylbutyrate(oxo) ruthenate(V)³⁵ were used, see Table 1. Energies for Ru K-edge reported in Table 1 were recorded halfway along the rising edge of normalized fluorescence spectra.

2.6. EXAFS Data Analysis. Athena software was used for data processing.³⁶ The energy scale for each scan was normalized by using ruthenium metal standard and scans for the same samples were added. Data in energy space were pre-edge corrected, normalized, deglitched (if necessary), and background corrected. The processed data were next converted to the photoelectron wave vector (k) space and weighted by k^3 . The electron wavenumber is defined as $k = [2m(E -$

$E_0)/\hbar^2]^{1/2}$, where E_0 is the threshold energy. k -space data were truncated near the zero crossings ($k = 3.904$ to 15.063 Å⁻¹) in Ru EXAFS before Fourier transformation. The k -space data were transferred into the Artemis Software for curve fitting. To fit the data, the Fourier peaks were isolated separately, grouped together, or the entire (unfiltered) spectrum was used. The individual Fourier peaks were isolated by applying a Hanning window to the first and last 15% of the chosen range, leaving the middle 70% untouched. Curve fitting was performed using ab initio calculated phases and amplitudes from the FEFF8 program from the University of Washington.³⁷ Ab initio calculated phases and amplitudes were used in the EXAFS equation:³⁸

$$\chi(k) = S_0^2 \sum_j \frac{N_j}{kR_j^2} f_{\text{eff}j}(\pi, k, R_j) e^{-2\sigma_j^2 k^2} e^{-2R_j/\lambda_j(k)} \times \sin(2kR_j + \phi_{ij}(k)) \quad (1)$$

where N_j is the number of atoms in the j th shell; R_j is the mean distance between the absorbing atom and the atoms in the j th shell; $f_{\text{eff}j}(\pi, k, R_j)$ is the ab initio amplitude function for shell j ; and the Debye–Waller term $e^{-2\sigma_j^2 k^2}$ accounts for damping due to static and thermal disorder in absorber-backscatterer distances. The mean free path term $e^{(-2R_j)/\lambda_j(k)}$ reflects losses due to inelastic scattering, where $\lambda_j(k)$ is the electron mean free path. The oscillations in the EXAFS spectrum are reflected in the sinusoidal term $\sin(2kR_j + \phi_{ij}(k))$, where $\phi_{ij}(k)$ is the ab initio phase function for shell j . This sinusoidal term shows the direct relation between the frequency of the EXAFS oscillations in k -space and the absorber-backscatterer distance. S_0^2 is an amplitude reduction factor.

The EXAFS equation (eq 1) was used to fit the experimental Fourier isolated data (q -space) as well as unfiltered data (k -space) and Fourier transformed data (R -space) using N , S_0^2 , E_0 , R , and σ^2 as variable parameters (see fit results in Tables 2, and S1–2 in the SI). N refers to the number of coordination atoms surrounding Ru for each shell. The quality of fit was evaluated by the R -factor and the reduced χ^2 value. The deviation in E_0 ought to be less than or equal to 10 eV. An R -factor less than 2% denotes that the fit is good enough whereas an R -factor between 2% and 5% denotes that the fit is correct within a consistently broad model.³⁹ The reduced χ^2 value is used to compare fits as more absorber-backscatter shells are included to fit the data. A smaller reduced χ^2 value implies a better fit. Similar results were obtained from fits done in k -, q -, and R -spaces. To determine the Ru–O–Ru bond angles, a model accounting for backscattering amplitude and phase shift of the Ru–O–Ru three atom system was created in FEFF. It is known that the focusing effect is mainly due to the backscattering amplitude, thus, fitting of the entire spectrum was done to optimize the Ru–O distance, the Ru–O–Ru coordination number, and the Debye–Waller factors. The experimental data were fitted for the range of Ru–O–Ru angles from 150° to 180° with 1° steps, Figure 3. A multiple scattering model with a Ru–O–Ru coordination number equal to 1 was determined to have the correct Ru–O–Ru angle. Additionally, the distance found for the Ru–O distance from multiple bond fitting of the Ru–O–Ru angle was the same as the Ru–O distance extracted by fitting the first peak only. This confirmed the accuracy of the fitting procedure.

2.7. Resonance Raman Measurements. Low-temperature Resonance Raman spectra were recorded by using a XploRa Horiba Raman microscope at 532 nm excitation. The samples were measured on a Linkam cryostage (100 K) connected to the microscope stage below the laser beam aperture. The sample and window space of the cryostage were continuously purged with nitrogen gas to avoid frost formation and enable easy focusing on the sample. Samples were measured with 10 mW laser excitation power. Scans were recorded with shortest 3 s exposure and no laser induced damage was observed in consecutive scans.

3. RESULTS

3.1. Validation of Ru K-Edge XAS: Analysis of the Blue Dimer Catalyst in Stable Oxidation States. Blue dimer catalysts with Ru centers in formal oxidation states [3,3] and [3,4] are stable. They can be prepared as microcrystalline solids or in solutions. X-ray structures of these complexes are available^{3,10} and the K-edge EXAFS was previously reported.³¹

Ru K-edge XANES of the blue dimer [3,3] and [3,4] have been reported³¹ but assignment of Ru oxidation states was not validated by comparison with model compounds. Figure 1

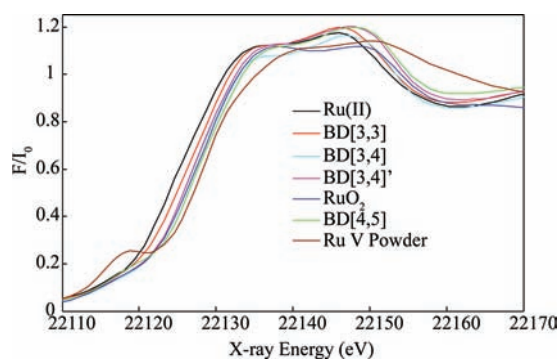


Figure 1. Normalized Ru K-edge XANES of the blue dimer in oxidation states [3,3] and [3,4] and its reactive intermediates [4,5] and [3,4]'. Reference compounds are Ru(II) complex: Ru(Mebimpy)-(bpy)(H₂O)](NO₃)₂ (where Mebimpy = 2,6-bis(1-methylbenzimidazol-2-yl)pyridine and bpy = 2,2'-bipyridine), RuO₂ and tetra-*n*-propylammonium bis-2-hydroxy-2-ethylbutyrato(oxo) ruthenate(V).

shows XANES spectra of the blue dimer [3,3] and [3,4] as well as spectra of a related Ru(II) complex and ruthenium(IV) oxide (RuO₂). The Ru K-edge XANES of the blue dimer [3,3] is consistent with assignment of the Ru oxidation state as Ru(III) (Figures 1 and S1 in the SI, Table 1). Analysis of the Ru L_{2,3}-

Table 1. Comparison of XANES Energy for Blue Dimer Catalysts

sample	edge energy (eV)	difference between current and previous rows
Ru(II) from monomeric complex	22123.93	
BD [3,3]	22125.01	1.08
BD[3,4]	22125.74	0.73
BD[3,4]'	22125.74	0
RuO ₂	22126.11	0.37
BD[4,5]	22126.45	0.34
Ru(V)	22127.15	0.70

edge XANES of the blue dimer [3,3] validated the same assignment.⁴⁰ One-electron oxidation of [3,3] with formation of [3,4] results in a pronounced Ru K-edge shift to higher energy. Thus, K-edge XANES has sufficient sensitivity to detect oxidation of one of two Ru centers in the blue dimer molecule. Figure 1 shows that the spectrum of [3,4] lies at lower energy compared to RuO₂ consistent with the assignment of the [3,4] oxidation state distribution for this complex.

Ru K-edge EXAFS spectra of stable blue dimer complexes were obtained from powders [((bpy)₂(H₂O)Ru)₂O](ClO₄)₄ and [((bpy)₂(H₂O)Ru)₂O](PF₆)₄ and for 0.5 mM solutions in 0.1 M HNO₃ measured at 20 K, Figures 2 and S2, SI. The EXAFS spectrum contains two prominent peaks: peak I

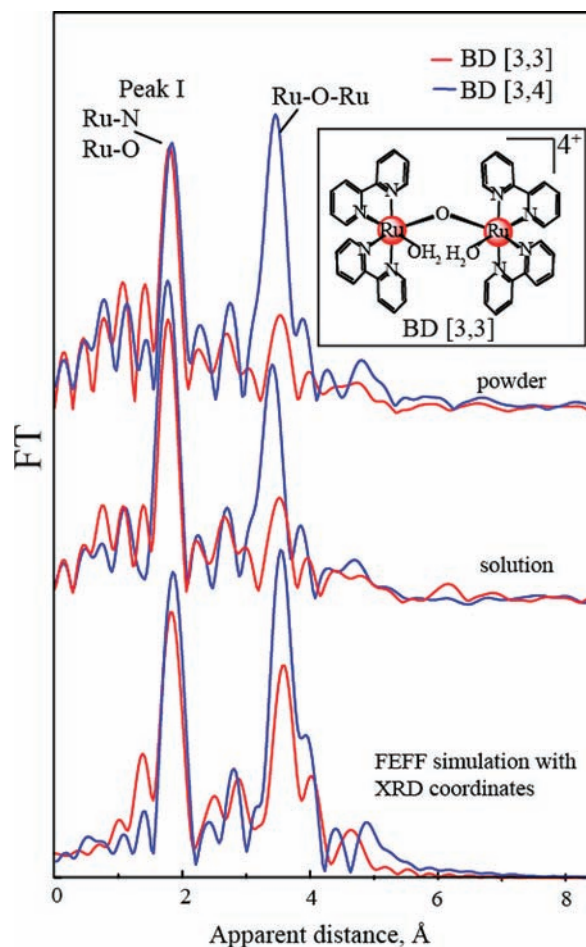


Figure 2. Fourier transforms of k^3 -weighted Ru EXAFS (Figure S2 in the SI) of the blue dimer in oxidation states [3,3] and [3,4] obtained from powders (A) and in 0.1 M HNO₃ solution (B). (C) EXAFS spectra simulated with FEFF software. Coordinates of all atoms from X-ray structures of [3,3] and [3,4]^{3,10} were used as input.

corresponding to the first coordination sphere including Ru–N and Ru–O interactions and the peak labeled “Ru–O–Ru” (Figure 2) above 3 Å corresponding to the apparent distance originating from the Ru–Ru interaction across the μ -oxo bridge. EXAFS fits for the first coordination sphere (peak I) and for the entire spectrum ($R = 1.3\text{--}3.6 \text{ \AA}^{-1}$) are in Tables 2 and S1 and Figures S2 and S3, SI. Analysis of peak I clearly resolves Ru–N interactions at 2.07 Å and bridging Ru–O distance at 1.86 Å (Tables 2 and S1, SI). However, experimental resolution is not sufficient to resolve the Ru–OH₂ interaction at 2.14 Å from the four Ru–N interactions at 2.1 Å. For instance, inclusion of the additional Ru–O shell in peak I fitting improves the fit as shown by decreased R -factors and χ^2 values, Table S1 in the SI, fits 2, 3 and 8, 9. However, when the fit is performed for the entire spectrum, addition of the extra Ru–O shell to model the Ru–OH₂ interaction does not result in improvement of the fit and accurate estimation of the Ru–OH₂ distance, Table S1 in the SI, fits 5, 6 and 11, 12. Thus, in Table 2, only average Ru–N/Ru–OH₂ interactions are listed. The similarity between light atoms O and N enabled this analysis without introducing significant errors. The same approach was used in an earlier EXAFS analysis of the blue dimer.³¹

Table 2. Comparison of Structural Parameter from EXAFS and XRD for Blue Dimer [3,3], [3,4], and [4,5]

species ^a	EXAFS ^b (shell: $N \times$ distance in Å)	XRD ^{3,10} (bond distances in Å)
blue dimer [3,3] fit #1 ^a	Ru–N: 5×2.07	Ru–N: 2.03, 2.05, 2.06, 2.09
	Ru–O: 1×1.86	Ru–O: 1.87
	Ru–C: 8×3.03	Ru–H ₂ O: 2.14
	Ru–O–Ru: $165 \pm 2^\circ$	Ru–O–Ru: 165.5°
	Ru–Ru: 1×3.69	Ru–Ru: 3.71
blue dimer [3,4] fit #24 ^a	Ru–N: 5×2.09	Ru ^{III}
	Ru–O: 1×1.83	Ru–N: 2.02, 2.05, 2.07, 2.10
	Ru–C: 8×3.00	Ru–O: 1.85
	Ru–O–Ru: $171 \pm 2^\circ$	Ru–H ₂ O: 2.15
	Ru–Ru: 1×3.67	Ru ^{IV}
		Ru–N: 2.06, 2.09, 2.10, 2.12
		Ru–O: 1.82
		Ru–OH: 1.98
		Ru–O–Ru: 170°
		Ru–Ru: 3.66
blue dimer [4,5] fit #31 ^a	Ru–N: 4×2.09	Ru ^V =O: 1.70 in Ru ^V reference compound ³⁵
	Ru–O: 1×1.87	Ru ^{IV} =O: 1.83; 1.81; 1.81 in complexes with amino ligands ^{39,42,43}
	Ru–O: 1×1.70	
	Ru–C: 8×3.02	
	Ru–O–Ru: $166 \pm 2^\circ$	
blue dimer [3,4] fit #26 ^a <i>R</i> -factor = 0.0051, reduced χ^2 = 35676	Ru–Ru: 1×3.71	
	Ru–N: 5×2.07	
	Ru–O: 1×1.85	
	Ru–C: 8×3.00	
	Ru–O–Ru: $164 \pm 2^\circ$	
Model 1: fit #28 ^a <i>R</i> -factor = 0.0025, reduced χ^2 = 23271	Ru–Ru: 1×3.66	
	Ru–N: 4×2.07	Ru–OO: 1.99–2.00 ^{54–59}
	Ru–O: 1×1.84	
	Ru–O: 1×1.93	
	Ru–O–Ru: $164 \pm 2^\circ$	
Model 2: fit #29 ^a <i>R</i> -factor = 0.0024, reduced χ^2 = 21948	Ru–Ru: 1×3.65	
	Ru–C: 8×2.99	
	Ru–N: 4×2.07	
	Ru–O: 1×1.84	
	Ru–O: 1.5×1.94	
	Ru–O–Ru: $164 \pm 2^\circ$	
	Ru–Ru: 1×3.65	
	Ru–C: 8×2.98	

^aSee Tables S1 and S2 in the SI for fit numbers. ^b N = number of vectors given per Ru center.

At pH 1, blue dimer [3,4] has water coordinated to Ru(III) with a Ru–O distance of 2.10 Å and a hydroxyl group coordinated to Ru(IV) with Ru–O 1.98 Å, see Table 2. Oxidation of one Ru center leads to a decrease of the Ru–O (bridge) distance from 1.86 Å in BD [3,3] to 1.83 Å in BD [3,4], which is in agreement with XRD data. Similar to fits of blue dimer [3,3], some of the EXAFS fits for blue dimer [3,4] solution allow an additional Ru–OH₂ interaction to be pinpointed at about 2.15 Å with $N = 0.5$ as this Ru–OH₂ interaction occurs at only one of the Ru centers, Table S1 in the SI, fits 22, 25, and 26. Contrary to fits of blue dimer [3,3], inclusion of an addition shell for the entire spectrum of BD [3,4] solution resolves the Ru–OH₂ interaction at 2.15 Å from the four Ru–N distances with improvement of the fit quality, Table S1 in the SI, fits 24 and 25.

Analysis of the EXAFS spectrum ($R = 1.3$ – 3.6 Å⁻¹) allows determination of the Ru–O–Ru bond angle, Figure 3, Tables 2 and S1 in the SI. Multiple scattering paths for the Ru–O–Ru unit are indicated in Figures 3 and S4 in the SI. A model accounting for backscattering amplitude and phase shift of the

Ru–O–Ru three-atom system was created in FEFF and used to determine Ru–O–Ru angles. It is known that the focusing effect is mainly due to the backscattering amplitude, thus, fitting of the entire spectrum was done to optimize the Ru–O distance, Ru–O–Ru coordination number, and Debye–Waller factors. The experimental data were fitted for the range of Ru–O–Ru angles from 150° to 180° with 1° steps, Figures 3 S4 in the SI. A multiple scattering model that resulted in a Ru–O–Ru coordination number equal to 1 was determined to have the correct Ru–O–Ru angle. Obtained angles are in close agreement with the earlier results of XRD studies, Table 2. No significant differences were obtained for the structures of the blue dimer [3,3] and [3,4] in powders versus solutions, Figures 3 and S4 and Table S1 in the SI. In summary, oxidation of the blue dimer from [3,3] to [3,4] leads to several significant structural changes such as shortening of the bridging Ru–O distance and flattening of the Ru–O–Ru angle. Changes detected in EXAFS correlate well with data from XRD analysis showing that this technique can be used reliably for analysis of unknown structures in the blue dimer catalytic sequence.

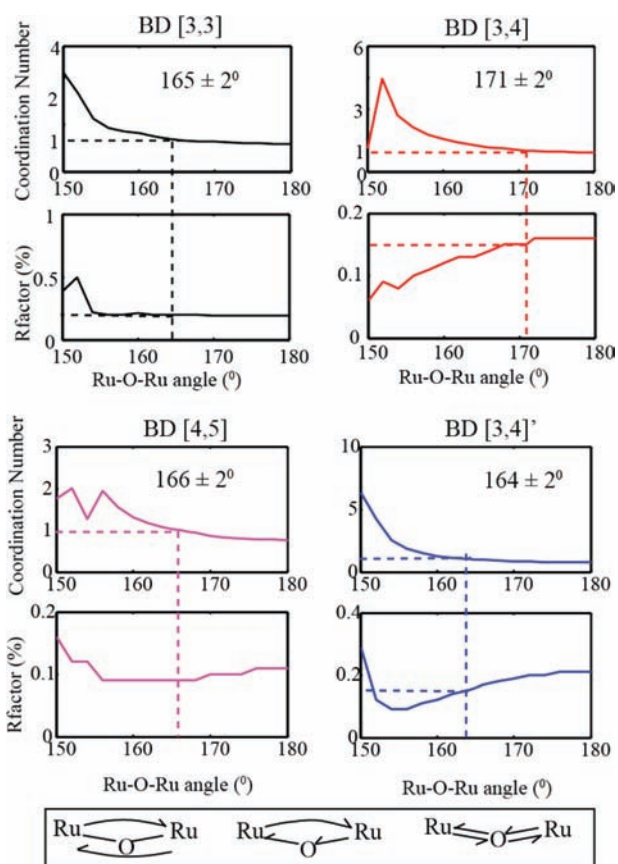


Figure 3. Result of the Ru–O–Ru angle determination for blue dimer [3,3]; [3,4] and oxidized intermediates [4,5] and [3,4]'. Coordination numbers are plotted as a function of the Ru–O–Ru angle. The angle is determined to be the one that provides accurate coordination number. Multiple scattering paths for the Ru–O–Ru unit are shown below.

3.2. EPR Analysis of the Reaction of Blue Dimer [3,4] with 2 and 3 Equiv of Ce(IV). Oxidation of blue dimer [3,4] with 2 and 3 equiv of Ce(IV) allows for a fractional or single turnover of the catalyst correspondingly. Kinetics of blue dimer [3,3] oxidation to [3,4] with Ce(IV) were studied earlier and a rate constant k of about 6×10^2 to $7 \times 10^2 \text{ M}^{-1} \text{ s}^{-1}$ at pH 1 was observed with only a slight dependence on the acid.¹² To avoid interference of this kinetic component, we used the [3,4] form of the blue dimer. Oxidation of blue dimer [3,4] with 1, 2, or 3 equiv of Ce(IV) resulted in decay of its absorption at 494 nm, Figure S5 in the SI, and decay of the EPR signal of blue dimer [3,4], Figure 4A. Decay of [3,4] follows complex kinetics with characteristic time dependent shifts in absorption maxima from 494 to 486 nm when 2 or 3 equiv was added or to 480 nm with addition of excess Ce(IV) (20 equiv), Figure S5 in the SI. Such UV–vis absorption kinetics are known to be complex and their interpretation has led to controversial results in the past.^{32,33}

Here we attempted to improve the information content of UV–vis absorbance measurements by parallel EPR analysis of reaction mixtures. Figure 4A shows the EPR spectra of the initial blue dimer [3,4] and reaction mixtures frozen within 30 s after addition of 1, 2, and 3 equiv of Ce(IV). Similar results were obtained for blue dimer concentrations in the range 0.25–1 mM and at EPR recording temperatures of 80 to 10 K. Figure 4A shows that while addition of 1 equiv of Ce(IV) is not sufficient to completely oxidize initial [3,4] (at least during 30

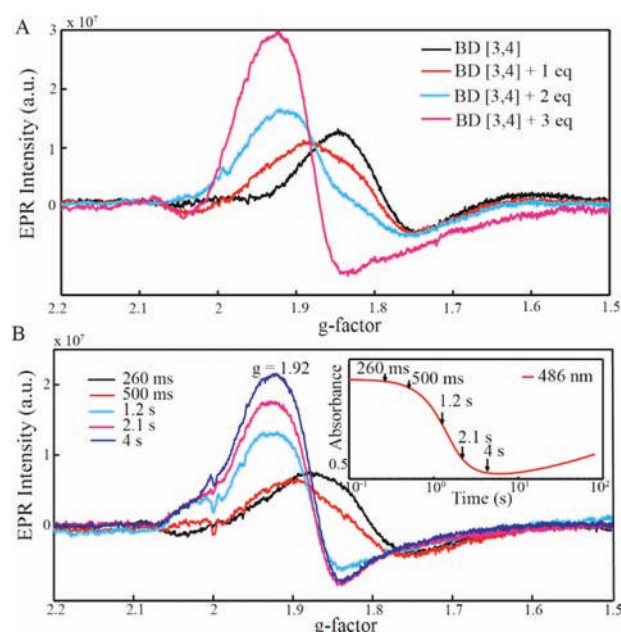


Figure 4. X-band EPR spectra (20 K) of 0.25 mM blue dimer [3,4] in 0.1 M HNO₃ after (A) addition of 1, 2, or 3 equiv of Ce(IV) and freezing within 30 s; (B) freeze quench preparation with addition of 2 equiv of Ce(IV) and freezing at indicated times. Inset: Stopped flow UV vis absorbance of [3,4] with 2 equiv of Ce(IV) at 486 nm.

s), addition of 2 equiv of Ce(IV) results in nearly complete oxidation, and 3 equiv provides complete conversion of [3,4] within 30 s (data are shown for 0.25 mM blue dimer). Oxidation of blue dimer [3,4] results in a new EPR signal with the maximum signal intensity at $g = 1.92$, Figure 4. We attribute this new EPR signal to an intermediate that has been termed [3,4]' as described below (see XAS analysis of oxidation states).

Time-dependent evaluation of the formation of this new EPR signal was carried out by parallel stopped-flow UV–vis absorption kinetic measurements and freeze-quenching of reaction mixtures for EPR analysis. The insert in Figure 4B shows characteristic changes in absorption upon oxidation of blue dimer [3,4] with arrows indicating times when samples were collected for EPR analysis. These experiments were repeated several times with similar results obtained.

Data in Figure 4B show that the main change in absorbance is accompanied by formation of a $g = 1.92$ EPR signal (1.2 s) and that this signal grows in intensity at longer times. Critically, after 500 ms, the EPR signal of the [3,4] starting material is no longer detectable while [3,4]' continues to grow in intensity. This suggests that BD [3,4]' cannot be a product of a direct conversion from BD [3,4]. The [3,4]' intermediate may originate from the reaction of an EPR silent intermediate, possibly BD [4,4], or transient [4,5] intermediate (section 3.4, Figure 8 below) with water. A weak shoulder on the low field side of the [3,4]' EPR signal (Figure 4B) might indicate a small contribution of the [4,5]. This shoulder is not visible in samples prepared by simple mixing (Figure 4A), which is in agreement with a short lifetime of the [4,5], section 3.4, Figure 8. No other signals but these plotted in Figure 4 were detected at other field positions or in parallel mode EPR.

Power and temperature dependences of the EPR signals for blue dimer [3,4] and $g = 1.92$ EPR signal of the [3,4] intermediate are shown in Figures S6 and S7 in the SI. Signals appear to have different relaxation behaviors and different

Curie constants. The intensity of the $g = 1.92$ EPR signal is about three times as large as that of blue dimer [3,4] from which it has been generated by oxidation. EPR was used to analyze the stability of the [3,4]' intermediate, Figure 5A.

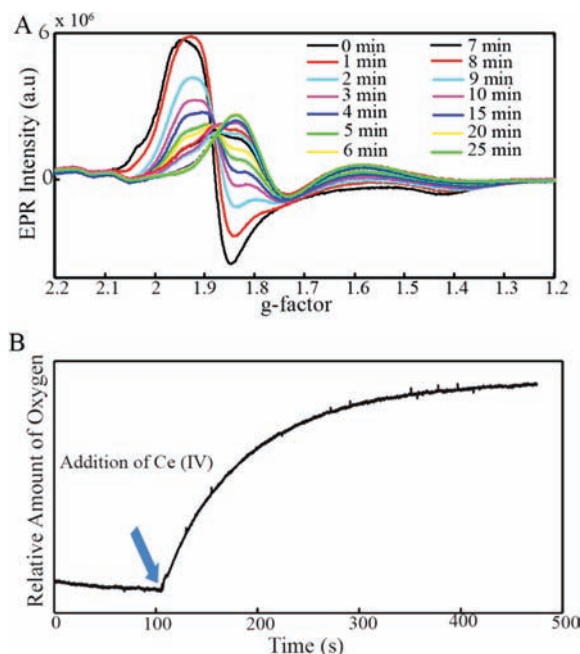


Figure 5. (A) Analysis of the stability of the [3,4]' intermediate by EPR. Samples of intermediate were prepared by adding 3 equiv of Ce(IV) to a 1 mM solution of blue dimer [3,4] in 0.1 M HNO₃. The samples were melted for the indicated period of time at room temperature and refrozen for EPR analysis at 20 K. (B) Kinetics of O₂ evolution recorded with oxygen electrode immersed into the solution of the blue dimer [3,3] (0.1 mM in 0.1 M HNO₃) after addition of 4 equiv of Ce(IV) to induce a single turnover.

Reaction mixtures containing the intermediate were melted to room temperature to allow the reaction to proceed further and then refrozen at different time intervals for EPR analysis. As shown in Figure 5A, the EPR signal at $g = 1.92$ converts completely to blue dimer [3,4] within 25 min at a concentration of 1 mM.

Careful analysis of the literature allowed us to identify that the intermediate detected here was noted for the first time in 1994 by Hurst and co-workers.²⁸ Its g -factor, however, was incorrectly reported as $g = 1.87$ and it was assigned to blue dimer [4,5]. This intermediate was observed by EPR in reaction mixtures of blue dimer [3,3] and Ce(IV) in 1 and 0.1 M CF₃SO₃H (addition of Ce(IV) up to 16 equiv carried out at +4 °C). Similar to this study, the intermediate was shown to return to [3,4] in 5–10 min at room temperature. This EPR signal was not investigated further at the time; however, with later studies it became clear that it does not arise from blue dimer [4,5] intermediate.²⁶

Competence of the detected [3,4]' intermediate for O₂ evolution was assessed by time-resolved O₂ evolution measurements with an oxygen electrode immersed in the reaction mixture (see Materials and Methods). Figure 5B shows the profile of O₂ evolution from a solution containing 0.1 mM blue dimer catalyst. To induce a single turnover, 4 equiv of Ce(IV) were added to activate blue dimer [3,3] catalyst. Under such conditions, [3,4]' is formed within a few seconds (see Figure 4) and persists in solution for some minutes. O₂ evolution

continued for about 5 min and resulted in evolution of 0.053 μmol of O₂, Figure 5B. The maximal rate of oxygen evolution within the first 30 s was 5.64×10^{-4} μmol of O₂/s. Thus, the time frame for observation of the [3,4]' was the same as the time frame for oxygen evolution. Highly oxidized [4,5] and [5,5] intermediates of the blue dimer are known to have distinct EPR signal.^{26,28,32} However, the EPR signal of the [3,4]' intermediate is predominant under conditions producing O₂ with an amount of Ce(IV) sufficient for a single turnover.

3.3. XANES, EXAFS, and Resonance Raman Analysis of the [3,4]' Samples obtained by oxidation with 3 equiv of Ce(IV) and frozen within 30 s show the maximum intensity of the new EPR signal, Figure 4A, and were thus analyzed by XAS at Ru K-edges. Figure 6 shows examples of parallel EPR and

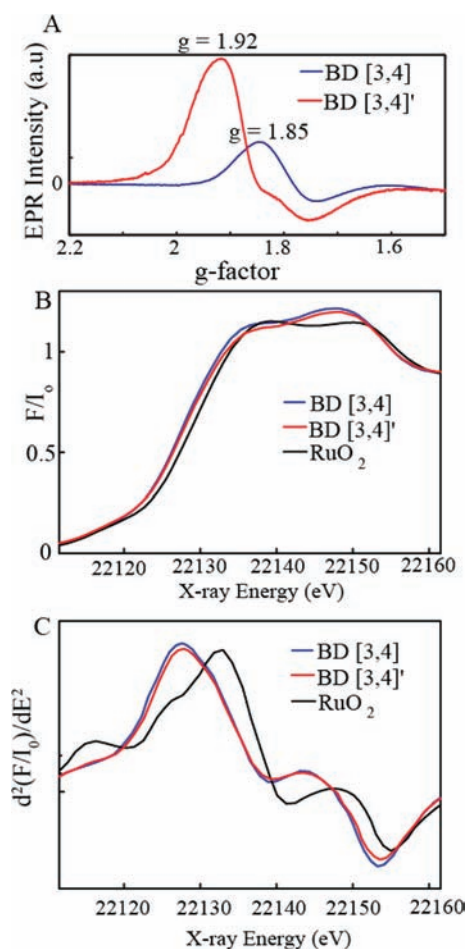


Figure 6. Comparison of spectroscopic characteristic of the blue dimer [3,4] and oxidized intermediate [3,4]': (A) X-band EPR spectra (20 K); (B) normalized Ru K-edge XANES including reference compound RuO₂; (C) second derivative of normalized Ru K-edge XANES.

XAS analysis. Frozen samples of the oxidized blue dimer intermediate did not demonstrate a shift in Ru K-edge XANES sufficient to account for oxidation of at least one Ru center. While the shape of the absorption edge is slightly different for the oxidized sample from BD [3,4] (Figure 6B), the absence of a shift is clear in the first derivative of the absorption edge of oxidized sample, Figure 6C. Thus, we assigned the oxidation state of Ru centers to [3,4] in the intermediate. This assignment is consistent with EPR results, which can be interpreted as an $S = 1/2$ resonance and it is similar in shape to

the EPR spectrum of the initial [3,4]. However, it shows a pronounced shift in g -tensor and differences in relaxation properties which led to its labeling as [3,4]'. The possible explanation for an absence of shift in the absorption edge under oxidizing conditions could be due to an oxidative modification of the ligand. The experiment shown in Figure 6 was repeated during 3 different beam times with freshly prepared samples and the same results were obtained. No X-ray induced damage was detected under the experimental conditions (20 K, defocused beam).

To analyze the ligand environment in [3,4]', its Ru K-edge EXAFS was recorded and shown in Figure 7A. Differences between [3,4] and [3,4]' are indicated by arrows. These differences were reproducibly obtained on six independently prepared samples measured during 3 different beam times. Measurements with ultra-low flux (10 times lower than conventionally used X-ray flux at the APS BM-20 beamline in

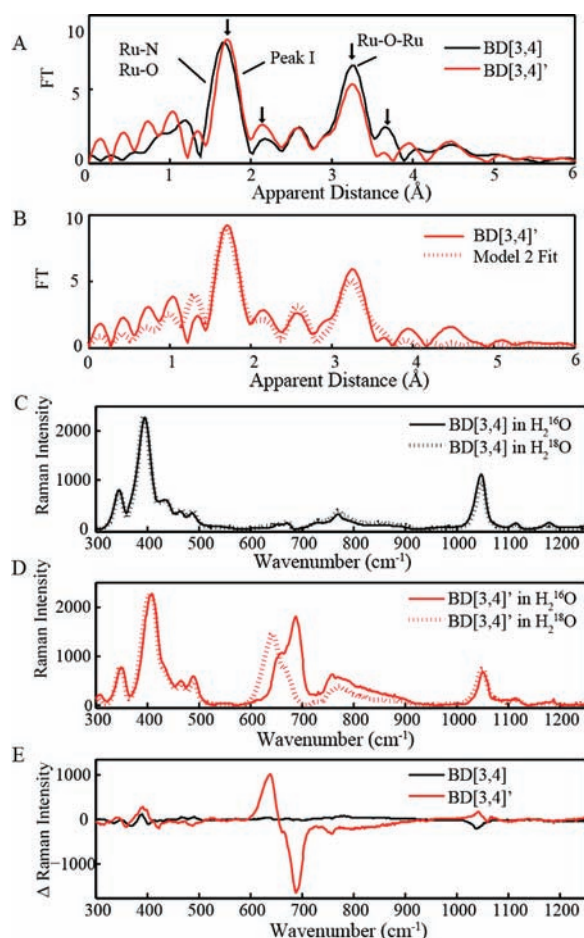


Figure 7. (A) Fourier transforms of k^3 -weighted Ru EXAFS (Figure S2, SI) of the blue dimer [3,4] and oxidized intermediate [3,4]'. (B) Comparison of the Fourier transforms of k^3 -weighted Ru EXAFS of the oxidized intermediate [3,4]' and result of the fit to Model 2 (Table 2). (C) Resonance Raman with excitation at 532 nm of the blue dimer [3,4] in regular and ^{18}O -enriched water recorded at 100 K. Sample is 1 mM [3,4] solution in 0.1 M HNO_3 . (D) Resonance Raman with excitation at 532 nm of the blue dimer [3,4]' intermediate prepared in regular and ^{18}O -enriched water and recorded at 100 K. Sample was generated by adding 2 equiv of the Ce(IV) to 1 mM [3,4] solution in 0.1 M HNO_3 and freezing within 30 s. (E) Difference spectra (100 K) obtained by subtracting BD [3,4] and BD[3,4]' spectra in regular water from those obtained in ^{18}O -enriched water.

defocused mode) resulted in the same EXAFS spectrum and indicated that EXAFS features are not affected by X-ray induced damage. EXAFS data in Figure 7 show that the Ru–O–Ru bridge remains intact in the intermediate. The peak corresponding to Ru–Ru interaction is in the same position; however, its intensity is lower indicating a change in the Ru–O–Ru angle. Peak I containing Ru first coordination sphere ligands (O, N) interactions appears modified and an additional peak of increased intensity is detected just above 2 Å in apparent distance. These changes indicate modification of the ligand environment in [3,4]' relative to [3,4].

Fitting of EXAFS data was performed in q -, k -, and R -spaces and similar results were obtained, see Tables 2 and S2, SI, and Figures 7B and S2, S3, and S8, SI. Fits of EXAFS data reliably resolve Ru–N interactions at about 2.07 Å and the Ru–O unit of μ -oxo bridge at 1.85 Å, Tables 2 and SI, and demonstrate that the Ru–O–Ru angle decreased from $171 \pm 2^\circ$ in [3,4] solution to $164 \pm 2^\circ$ in the [3,4]' intermediate (Figure 3, Table 2). Intriguingly, to account for the experimentally observed increase in EXAFS intensity just above 2 Å in apparent distance, an additional Ru–O interaction at 2.55 Å can be introduced into EXAFS fits resulting in the improved fit qualities (Table S2, SI). While some of the [3,3] and [3,4] Fourier transformed EXAFS spectra (Figure 2) also show weak peaks around that apparent distance, fits to these data do not improve upon introduction of the Ru–O vector at 2.6 Å, Table S1, SI. However, the information derived from EXAFS analysis is not sufficient to identify the unknown structure of the intermediate.

Resonance Raman with excitation at 532 nm was used to analyze the possibility that the [3,4]' intermediate contains a peroxo ligand. Measurements were done on frozen solutions of the BD [3,4] and [3,4]' intermediates at 100 K, Figure 7C,D,E. The resonance Raman spectrum of BD [3,4] is in agreement with previous reports.^{29,32} The main spectral feature at 397 cm^{-1} corresponds to the symmetric Ru–O–Ru stretching mode.²⁹ Raman spectra of the BD [3,4] prepared in the regular and in the ^{18}O -enriched (98%) water are almost identical (Figure 7C,E) showing that the bridging oxygen is not exchanged under experimental conditions and that Ru–OH₂ and Ru–OH modes are not visible in the Raman spectrum as has been previously demonstrated.²⁹ Spectra of the [3,4] intermediate prepared in the regular and ^{18}O -enriched water demonstrated a prominent shift of the band at 683 cm^{-1} to 637 cm^{-1} (Figure 7D). A 46 cm^{-1} shift upon isotopic substitution is typical for the O–O bond stretch, see summary in ref 41. Data shown in Figure 7D,E are similar to those reported previously by Hurst (see Figure 8 in ref 32). At that time, changes in

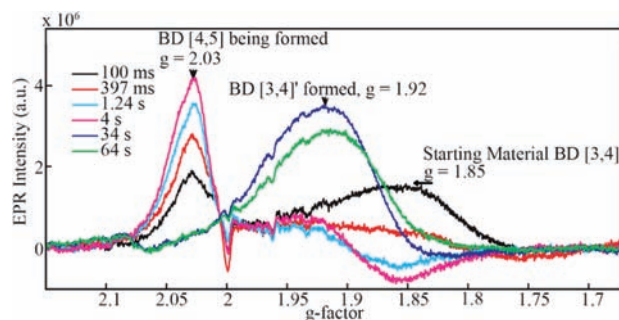


Figure 8. Results of freeze quench analysis of 0.25 mM blue dimer [3,4] in 0.1 M HNO_3 mixed with 20 equiv of Ce(IV).

Raman spectra were attributed to association between the BD [5,5] and Ce ions while explanation of the large isotopic shift of the 683 cm^{-1} band was not given.³² Our XAS data clearly show that the sample contains BD with Ru centers in oxidation states [3,4] and species with the 683 cm^{-1} band are detected in dilute solutions (1 mM as well as 0.5 mM BD concentrations) with only 2–3 equiv of Ce(IV). This rules out the earlier assignment of this band to blue dimer [5,5]. A distinct feature of the observed O–O band is its relatively low frequency (683 cm^{-1}); O–O vibration is typically expected to be in the $800\text{--}850\text{ cm}^{-1}$ for peroxides.

3.4. EPR and XAS Analysis of the Reaction of Blue Dimer [3,4] with an Excess of Ce(IV). Surprised by the absence of EPR and XANES spectroscopic signatures of the highly oxidized intermediates under single turnover conditions, we analyzed reaction mixtures of the blue dimer [3,4] with an excess (20 equiv) of Ce(IV) in 0.1 M HNO_3 . Figure 8 shows an EPR spectrum of the reaction mixture freeze-quenched at defined times after mixing. At very early times (100 ms to 4 s), the EPR spectrum assigned earlier to the [4,5] intermediate²⁶ was detected, Figures 8 and 9. However, this signal persists only for very short (up to 10 s) times in the reaction before giving way to the EPR signal of [3,4]'. The sample continues to evolve oxygen after the first 10 s, but only the [3,4]' intermediate is

detectable in the reaction mixture by EPR. This intermediate slowly converts back to [3,4] on the minutes time scale, thus completing the catalytic cycle, Figure 8.

Ru K-edge XANES measurements were used to analyze oxidation states of Ru centers in the blue dimer samples with the characteristic EPR signal assigned previously to [4,5]. Figure 9B shows Ru K-edge XANES of such sample compared with [3,4] starting material and the stable Ru(V) reference compound. Ru K-edge spectra of the oxidized intermediate is considerably shifted to higher energy as compared with [3,4] starting material, but at lower energy than the Ru(V) reference compound. The Ru(V) reference compound also displays a strong pre-edge. The pre-edge of the oxidized intermediate is higher than in [3,4] but not as high as in the reference compound. Thus, assignment of the [4,5] oxidation state is plausible and is in agreement with an earlier interpretation of the EPR signal.²⁶

EXAFS spectra of the [3,4] starting material and [4,5] intermediate are compared in Figure 9C. Oxidation results in a decrease in the intensity of the first EXAFS peak and a small shift of the peak corresponding to Ru–Ru interaction towards longer distance. Thus, EXAFS data indicate a change in the first coordination sphere of Ru ligands and an intact Ru–O–Ru bridge. The Ru–O–Ru angle in the oxidized intermediate ($166 \pm 2^\circ$) remained similar to the one in blue dimer [3,4], see Tables 2 and S1, S1, and Figure 3. To examine whether the presence of the short Ru–O interaction is responsible for broadening and reduced intensity of peak I we introduced a third Ru–O shell into EXAFS fits. This resulted in improved fit qualities, Table S1 in the SI, with a Ru–O distance of 1.70 Å. It is well within the range of Ru=O bond distances expected for Ru(V)=O³⁵ and Ru(IV)=O^{39,42,43} bonds, Table 2.

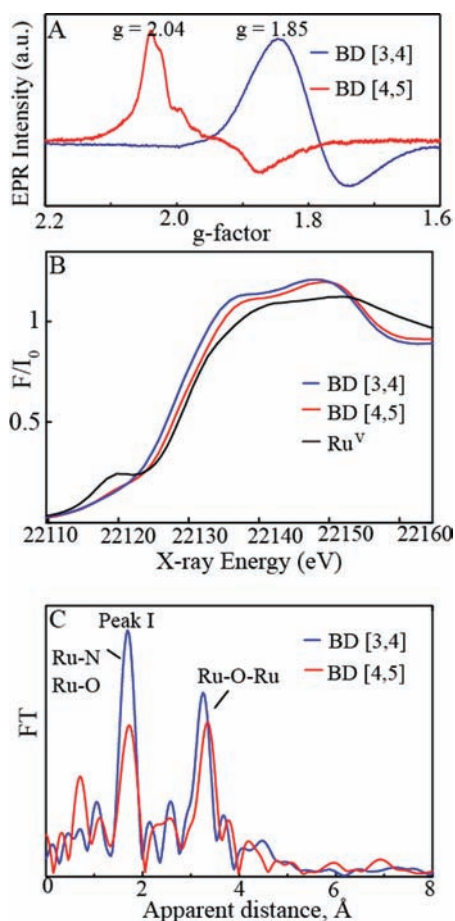


Figure 9. (A) Comparison of spectroscopic characteristic of blue dimer [3,4] and oxidized intermediate [4,5]: (A) X-band EPR spectra (20 K); (B) normalized Ru K-edge XANES including reference compound for Ru(V)=O: tetra-*n*-propylammonium bis-2-hydroxy-2-ethylbutyrate(oxo) ruthenate(V); (C) Fourier transforms of k^3 -weighted Ru EXAFS (Figures S2 and S3, SI).

4. DISCUSSION

4.1. Catalytic Cycle. Combined data from UV–visible stopped-flow and O_2 evolution analysis show that oxidation of blue dimer [3,4] by Ce(IV) occurs on the 100 ms to 1–2 s time scale (depending on concentrations of catalyst and oxidant). However, O_2 evolution proceeds on a time scale of minutes. Detailed spectroscopic analysis by EPR and XAS presented here demonstrates that highly oxidized species are formed at very short times (seconds) following blue dimer oxidation; however, they do not persist in solutions (even in dilute ones) at spectroscopically detectable concentrations at later times when the catalyst continues to evolve oxygen. Instead, a different short-lived intermediate, stable on the minutes time scale, is a dominant form of the catalyst in this condition consistent with the earlier observations.^{12,34}

The results obtained from these studies are summarized in the scheme shown in Figure 10B. Rates of reactions along the black arrows depend on the concentration of the oxidant (Ce(IV) in this study), while reaction with water (red arrow) is independent of the oxidant concentration. Thus, by using different Ce(IV) concentrations, different transient intermediates can be attained. Our experiments demonstrate that the [3,4]' intermediate is predominantly obtained by using low (2–3 equiv) Ce(IV) concentrations. In 0.1 M HNO_3 water oxidation is rapid, oxidation of the peroxo intermediate is slow, and the latter dominates at the catalytic steady state.¹²

4.2. [4,5] Intermediate. In blue dimer catalysts, oxidation states [4,5] and [5,5] have been characterized to a certain extent previously^{12,26,28,32,33} and in this work. We have not observed spectroscopic signatures of BD [5,5] which might be

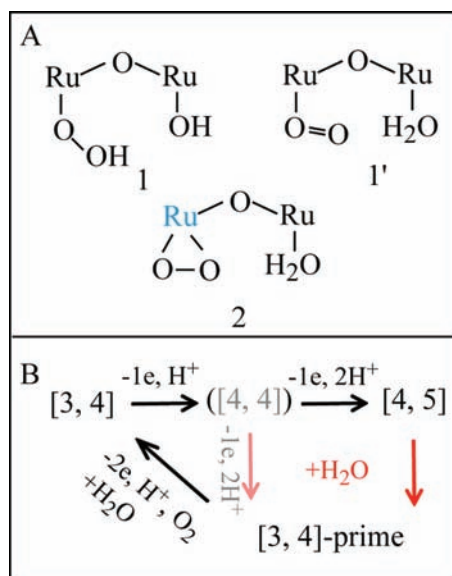


Figure 10. (A) Possible structures of the peroxides in the blue dimer molecule. (B) Scheme of the reactivity of the blue dimer [3,4] oxidized by Ce IV consistent with current study. Previously developed scheme of the blue dimer reactivity can be found in ref 13, Scheme 4.

due to its known rapid rate of water oxidation.³³ As noted above, the blue dimer [4,5] intermediate is known to be thermodynamically unstable. Previously it was generated by electrolysis at pH 7 at a potential of 1.2 V and by hypochlorite oxidation in phosphate buffer. Its Raman spectrum contained a 796 cm⁻¹ band assigned to the mode of a Ru=O bond and the EPR spectrum had characteristic components at 2.038, 2.012, and 1.895.²⁶ We demonstrated that the [4,5] intermediate can be detected in 0.1 M HNO₃ at very early times after addition of the oxidant. XAS analysis confirmed earlier assignment of reported EPR signal to [4,5] intermediate and the presence of a short Ru=O distance in the [4,5] blue dimer. The EXAFS analysis presented here is a first structural characterization of this molecule, which, as noted above, is reactive toward formation of the O–O bond and oxygen evolution.

4.3. [4,4] Intermediate. The rise time of [3,4]' upon addition of 2 equiv of Ce(IV) to blue dimer [3,4] in 0.1 M HNO₃ has a short lag time from disappearance of the [3,4] starting form of the catalyst. EPR data in Figure 4 show that [3,4]' is appearing while [3,4] is no longer detectable. The intermediate state between [3,4] and [3,4]' appears to be a short-lived [4,4] state, Figure 10B. Electrocatalyzed water oxidation by a surface-bound functionalized [Ru(bpy)₃]²⁺ has been suggested to occur by electron transfer catalysis with formation of the [4,4] intermediate.³⁴ Formation of this EPR silent intermediate could explain the rise in intensity of the [3,4]' EPR signal as it forms from the EPR silent state, Figure 4B. We cannot exclude participation of the [4,5] intermediate at a low (5–10% from EPR analysis) steady state level under these conditions. On the basis of electrochemical measurements [4,4] is an unstable oxidation state from pH 0–14. It does appear as a kinetic intermediate in the oxidation of [3,4] by Ce(IV).³⁴ Analysis of [4,4] is challenging and may not be possible. Pulsed radiolysis was used to generate a short-lived [4,4] intermediate and this intermediate was reported to be unstable above pH 2.²⁶ Reactivity toward water oxidation by other Ru(IV) moieties is known.^{41,44} Thermodynamically, [4,4] is the powerful oxidant and is highly unstable toward

disproportionation.¹² Although Hurst and co-workers have suggested that a [4,4] intermediate is stable and can be generated by mixing equal amounts of the electrochemically prepared blue dimer [5,5] and [3,3] ions, the actual nature of the intermediate is unknown and stabilization by anation may be important.³²

4.4. [3,4]' Intermediate. Our label for intermediate [3,4]' is based on EPR and XAS spectroscopic characteristics. Interestingly, it is generated under strongly oxidizing conditions, but does not show evidence for oxidation of the Ru centers from Ru XANES and EPR results. One possible explanation is that the intermediate contains an oxidized ligand. We explore possible ligand oxidation in [3,4]'. Bipyridine is known to be relatively stable toward oxidation under the conditions of the reaction, at least at early times. Oxidatively modified ligands derived from an acid anion are excluded as the same EPR spectra were obtained in different acids and the acids used are very stable toward oxidation. Given the coordination environment, the most reasonable explanation for an oxidized ligand or ligands is peroxide derived from coordinated hydroxide or water as suggested earlier.¹² Although logical, this explanation requires experimental confirmation.

We have so far been unsuccessful in using ESI-MS to characterize the [3,4]' intermediate as aqueous solutions provide poor ionization environments⁴⁵ resulting in cleavage of the μ -oxo bridge of the blue dimer under all conditions tested. EXAFS data suggest that there are no short Ru–O distances in [3,4]', which makes its structure different from the structure of BD [4,5]. From EXAFS, identification of the peroxide ligand is complicated by the fact that Ru–OH and Ru–OOH ligands are expected to have similar Ru–O bond distances at about 1.98–2.04 Å. Resonance Raman measurements give strong support for the presence of the O–O stretch by detecting a new vibration band in [3,4]' that undergoes a 46 cm⁻¹ downward shift upon ¹⁶O/¹⁸O exchange.

Different possibilities for peroxide coordination in the blue dimer are summarized in Figures 10A and S10, SI. Structures 1, 1', and 2 assume coordination at a single Ru center, Figure 10A, while 3–5 and 5' involve the Ru–O–Ru bridge, Figure S10 in the SI. On the basis of EXAFS data, structures 3–5 and 5' were determined to be less likely. For instance, structure 3 is very unlikely as it would imply a much smaller Ru–O–Ru angle than the Ru–O–Ru angle detected at 164 ± 2° in EXAFS fits (Tables 2 S2, SI). This structure is also unlikely based on analysis of ¹⁸O blue dimer water oxidation, which shows negligible production of ¹⁸O=¹⁸O dioxygen.²⁵ Peroxides similar to structure 5 are known for Pd,⁴⁶ Rh,⁴⁷ Mo,⁴⁸ Co,⁴⁹ and Fe/Cu complexes.⁵⁰ Structures similar to 4 have been found in Co,⁵¹ Cu,⁵² and Mo compounds,⁵³ although they all contained a second stabilizing bridge and are not structurally homologous to structure 4. For structures 4, 5, and 5' one can expect elongation of the Ru–O bridging distance due to the formation of the peroxo bridging ligand.^{46–53} However, EXAFS analysis shows that Ru–O bridge distance is almost unchanged. Analysis of the isotopically labeled μ -oxo-bridge of the blue dimer, under catalytic conditions, demonstrates that it remains intact under multiple turnovers of the catalyst.³² Our EXAFS data also show that the μ -oxo-bridge is intact in all analyzed intermediates of the blue dimer. Thus, we do not invoke reactivity of the μ -oxo-bridge oxygen in the formation of dioxygen.

This leaves us with Models 1, 1', and 2 as possible structures for [3,4]'. We evaluated the compatibility of Models 1–2 with

EXAFS data by doing EXAFS fits with structural elements of the Models 1–2, see Tables 2 and S2 (SI) and Figures 7B and S8 (SI). The seven-coordinated Ru center in Model 2 was accounted for by including an additional Ru–O interaction with $N = 0.5$. Inclusion of the additional shell of Ru–O in the first coordination sphere resulted in improved fits, see Tables 2 and S2 (SI). The Ru–O distance obtained in the analysis is in agreement with the expected 1.9–2.0 Å distance for the Ru–OO bond. However, resolution and precision (in terms of the analysis of N -numbers of Ru-backscatterer interactions) of the EXAF techniques are insufficient to distinguish between the Models. For Model 1, a change in frequency of the O–O vibration is expected when D₂O is used instead of H₂O. Such a shift was not observed here, Figure S9 in the SI, nor in an earlier analysis by Hurst.³² Model 1' contains the superoxide ligand with an electron effectively transferred from the peroxy O–O moiety to a Ru center with reduction of the Ru^{III}–Ru^{IV} moiety to Ru^{III}–Ru^{III}. The vibration for the O–O bond in superoxide is expected to occur at higher frequencies (1000–1200 cm⁻¹) due to the shorter O–O bond length and higher bond order that also contradicts the quite low frequency for O–O vibration detected here. These arguments leave Model 2 as the most likely candidate. Ru(II) complexes with a side-on peroxide group are well-known and have been previously characterized by XRD and Raman^{54–59} showing the O–O vibrations of 870–920 cm⁻¹.

To reconcile the discrepancy between the expected frequency of the O–O vibration and experimentally detected intense band at 683 cm⁻¹, we attempted DFT analysis of Raman activities and frequencies for BD molecule with Model 2 structure optimized by DFT, see Table S4 in the SI. While the predictive power of DFT for absolute values of frequencies is known to be poor, the qualitative insight from such analysis was still useful. The DFT analysis predicted an O–O vibration at 1069 cm⁻¹ but with a low Raman cross-section. However, two other coupled vibrations involving both Ru–OO and Ru–O(bridge) bonds were predicted to occur in the 600 cm⁻¹ range and have high Raman activities. The Raman data can be reconciled by proposing that the intense band at 683 cm⁻¹ is likely a coupled Ru–OO/Ru–O(bridge) vibration as shown in Table S4, SI. As both Ru–O(1) and Ru–O(2) vibrations contribute to this coupled mode, an isotopic shift of 46 cm⁻¹ is within the expected range. Detailed resonance Raman analysis and comparison with DFT results will be presented elsewhere.

5. CONCLUSIONS

Correlated UV–vis stopped-flow, EPR, XAS, and O₂ evolution measurements on the blue dimer water oxidation catalyst oxidized through single and multiple catalytic turnovers resulted in characterization of a new reactive intermediate [3,4]' and the previously described blue dimer [4,5]. During O₂ evolution at pH 1, most of the blue dimer catalyst exists as [3,4]' suggesting that it is either the active form of the catalyst or a key intermediate where oxidation is a rate limiting reaction under the conditions of the experiment. This intermediate has a different EPR spectrum with different relaxation properties compared to those of the stable [3,4] precursor. EPR and X-ray absorption near edge structure (XANES) are consistent with the assignment of oxidation states III and IV to the Ru centers in [3,4]'. However, a minimum number of 2 oxidizing equivalents are needed to generate this intermediate from blue dimer [3,4]. EPR and XAS spectroscopic characteristics of [3,4]' are significantly different from blue dimer [4,5], which is

also a 2 electron oxidation product of blue dimer [3,4] characterized in this study. EXAFS analysis demonstrates considerably modified ligand environments in [3,4]' and [4,5] intermediates. Raman measurements give strong support for the presence of the O–O stretch in [3,4]', which undergoes a 46 cm⁻¹ shift upon ¹⁶O and ¹⁸O exchange. Information obtained here about structure and electronic states of key intermediates helps further the analysis of the reaction mechanism by DFT and may contribute to catalyst optimization for better performance.

■ ASSOCIATED CONTENT

Supporting Information

Additional information is available on XAS, EPR, and UV–vis absorbance analysis of the blue dimer catalysts [3,3], [3,4], [3,4]', and [4,5]. This material is available free of charge via the Internet at <http://pubs.acs.org>.

■ AUTHOR INFORMATION

Corresponding Author

*ypushkar@purdue.edu, +1 (765) 496-3279

Present Address

#Currently at the University of California, Berkeley.

Notes

The authors declare no competing financial interest.

■ ACKNOWLEDGMENTS

Use of the Advanced Photon Source, an Office of Science User Facility operated for the U.S. Department of Energy (DOE) Office of Science by Argonne National Laboratory, was supported by the U.S. DOE under Contract No. DE-AC02-06CH11357. We thank Dr. Steve Heald and Dr. Dale Brewe for help with experiments at Beamline BM-20, APS. D.M. was partially supported by a Purdue Research Foundation grant. We thank the U.S. Department of Energy, Office of Basic Energy Sciences for financial support of this work under grant numbers DE-FG02-10ER16184 (Y.P.) and DE-FG02-06ER15788 (T.M.). Synthesis and characterization (J.J.C.) were supported by the UNC EFRC: Solar Fuels and Next Generation Photovoltaics, an Energy Frontier Research Center funded by the U.S. Department of Energy, Office of Science, Office of Basic Energy Sciences under Award Number DE-SC0001011. Access to EPR was provided by the Amy Instrumentation Facility, Department of Chemistry under supervision of Dr. Michael Everly. We also thank Gregory Robison for help with experiments at the beamline. We thank Dr. William Cramer and Dr. Stanislav Zakharov from structural biology at Purdue University for providing access to the SX20 Stopped-Flow UV–vis spectrometer (Applied Photophysics Ltd) and Dr. Yong Chen from the Department of Physics at Purdue University for allowing us to use the Xplora HORIBA Raman Microscope.

■ REFERENCES

- (1) Wydrzynski, T.; Satoh, S. *Photosystem II: The Light-Driven Water:Plastoquinone Oxidoreductase*; Springer: Dordrecht, The Netherlands, 2005.
- (2) Lewis, N. S.; Nocera, D. G. *Proc. Natl. Acad. Sci. U.S.A.* **2007**, *104* (50), 20142.
- (3) Schoonover, J. R.; Ni, J. F.; Roecker, L.; Whiter, P. S.; Meyer, T. J. *Inorg. Chem.* **1996**, *35* (20), 5885–5892.
- (4) Sartorel, A.; Carraro, M.; Toma, F. M.; Prato, M.; Bonchio, M. *Energy Environ. Sci.* **2011**, *5* (2), 5592–5603.

- (5) Sato, J.; Saito, N.; Yamada, Y.; Maeda, K.; Takata, T.; Kondo, J. N.; Hara, M.; Kobayashi, H.; Domen, K.; Inoue, Y. *J. Am. Chem. Soc.* **2005**, *127* (12), 4150–4151.
- (6) Kadowaki, H.; Saito, N.; Nishiyama, H.; Kobayashi, H.; Shimodaira, Y.; Inoue, Y. *J. Phys. Chem. C* **2007**, *111* (1), 439–444.
- (7) Morris, N. D.; Suzuki, M.; Mallouk, T. E. *J. Phys. Chem. A* **2004**, *108* (42), 9115–9119.
- (8) (a) Jiao, F.; Frei, H. *Angew. Chem.-Int Ed.* **2009**, *48* (10), 1841–1844. (b) Kanan, M. W.; Nocera, D. G. *Science* **2008**, *321* (5892), 1072–1075.
- (9) Hurst, J. K.; Cape, J. L.; Clark, A. E.; Das, S.; Qin, C. Y. *Inorg. Chem.* **2008**, *47* (6), 1753–1764.
- (10) Gilbert, J. A.; Eggleston, D. S.; Murphy, W. R.; Geselowitz, D. A.; Gersten, S. W.; Hodgson, D. J.; Meyer, T. J. *J. Am. Chem. Soc.* **1985**, *107* (13), 3855–3864.
- (11) Gersten, S. W.; Samuels, G. J.; Meyer, T. J. *J. Am. Chem. Soc.* **1982**, *104* (14), 4029–4030.
- (12) Liu, F.; Concepcion, J. J.; Jurss, J. W.; Cardolaccia, T.; Templeton, J. L.; Meyer, T. J. *Inorg. Chem.* **2008**, *47* (6), 1727–1752.
- (13) Deng, Z. P.; Tseng, H. W.; Zong, R. F.; Wang, D.; Thummel, R. *Inorg. Chem.* **2008**, *47* (6), 1835–1848.
- (14) Romero, I.; Rodriguez, M.; Sens, C.; Mola, J.; Kollipara, M. R.; Francas, L.; Mas-Marza, E.; Escriche, L.; Llobet, A. *Inorg. Chem.* **2008**, *47* (6), 1824–1834.
- (15) Zong, R.; Thummel, R. P. *J. Am. Chem. Soc.* **2005**, *127* (37), 12802–12803.
- (16) Tseng, H. W.; Zong, R.; Muckerman, J. T.; Thummel, R. *Inorg. Chem.* **2008**, *47* (24), 11763–11773.
- (17) Sartorel, A.; Carraro, M.; Scorrano, G.; De Zorzi, R.; Geremia, S.; McDaniel, N. D.; Bernhard, S.; Bonchio, M. *J. Am. Chem. Soc.* **2008**, *130* (15), 5006–5007.
- (18) Geletii, Y. V.; Botar, B.; Koegerler, P.; Hillesheim, D. A.; Musaev, D. G.; Hill, C. L. *Angew. Chem.-Int. Ed.* **2008**, *47* (21), 3896–3899.
- (19) Howells, A. R.; Sankarraj, A.; Shannon, C. *J. Am. Chem. Soc.* **2004**, *126* (39), 12258–12259.
- (20) McDaniel, N. D.; Coughlin, F. J.; Tinker, L. L.; Bernhard, S. *J. Am. Chem. Soc.* **2008**, *130* (1), 210–217.
- (21) Concepcion, J. J.; Jurss, J. W.; Templeton, J. L.; Meyer, T. J. *J. Am. Chem. Soc.* **2008**, *130* (49), 16462–16463.
- (22) Concepcion, J. J.; Tsai, M. K.; Muckerman, J. T.; Meyer, T. J. *J. Am. Chem. Soc.* **2010**, *132* (5), 1545–1557.
- (23) Concepcion, J. J.; Jurss, J. W.; Norris, M. R.; Chen, Z. F.; Templeton, J. L.; Meyer, T. J. *Inorg. Chem.* **2010**, *49* (4), 1277–1279.
- (24) Chen, Z.; Concepcion, J. J.; Hull, J. F.; Hoertz, P. G.; Meyer, T. J. *Dalton Trans.* **2010**, 39 (30), 6950–6952.
- (25) Yamada, H.; Siems, W. F.; Koike, T.; Hurst, J. K. *J. Am. Chem. Soc.* **2004**, *126* (31), 9786–9795.
- (26) Cape, J. L.; Lyman, S. V.; Lightbody, T.; Hurst, J. K. *Inorg. Chem.* **2009**, *48* (10), 4400–4410.
- (27) Hurst, J. K. *Coord. Chem. Rev.* **2005**, *249* (34), 313–328.
- (28) Lei, Y. B.; Hurst, J. K. *Inorg. Chem.* **1994**, *33* (20), 4460–4467.
- (29) Hurst, J. K.; Zhou, J.; Lei, Y. *Inorg. Chem.* **1992**, *31* (6), 1010–1017.
- (30) Yang, X.; Baik, M. H. *J. Am. Chem. Soc.* **2006**, *128* (23), 7476–7485.
- (31) Okamoto, K.; Miyawaki, J.; Nagai, K.; Matsumura, D.; Nojima, A.; Yokoyama, T.; Kondoh, H.; Ohta, T. *Inorg. Chem.* **2003**, *42* (26), 8682–8689.
- (32) Yamada, H.; Hurst, J. K. *J. Am. Chem. Soc.* **2000**, *122* (22), 5303–5311.
- (33) Binstead, R. A.; Chronister, C. W.; Ni, J. F.; Hartshorn, C. M.; Meyer, T. J. *J. Am. Chem. Soc.* **2000**, *122* (35), 8464–8473.
- (34) Jurss, J. W.; Concepcion, J. C.; Norris, M. R.; Templeton, J. L.; Meyer, T. J. *Inorg. Chem.* **2010**, *49* (4), 1277–1279.
- (35) Dengel, A. C.; Griffith, W. P.; Omahoney, C. A.; Williams, D. J. *J. Chem. Soc.-Chem Commun.* **1989**, 22, 1720–1721.
- (36) Ravel, B.; Newville, M. J. *Synchrotron Radiat.* **2005**, *12*, 537–541.
- (37) Rehr, J. J.; Albers, R. C. *Rev. Mod. Phys.* **2000**, *72* (3), 621–654.
- (38) Koningsberger, D. C.; Prins, R. *X Ray Absorption: Principles, Applications, Techniques of EXAFS, SEXAFS and XANES*; John Wiley & Sons, New York, 1988.
- (39) Cheng, W.-C.; Yu, W.-Y.; Zhu, J.; Cheung, K.-K.; Peng, S.-M.; Poon, C.-K.; Che, C.-M. *Inorg. Chim. Acta* **1996**, *242* (12), 105–113.
- (40) Alperovich, I.; Smolentsev, G.; Moonshiram, D.; Jurss, J. W.; Concepcion, J. J.; Meyer, T.; Soldatov, A.; Pushkar, Y. *J. Am. Chem. Soc.* **2011**, *133* (39), 15786–15794.
- (41) Polyansky, D. E.; Muckerman, J. T.; Rochford, J.; Zong, R.; Thummel, R. P.; Fujita, E. *J. Am. Chem. Soc.* **2011**, *133* (37), 14649–14665.
- (42) Cheng, W.-C.; Yu, W.-Y.; Cheung, K.-K.; Che, C.-M. *J. Chem. Soc., Dalton Trans.* **1994**, 1, 57–62.
- (43) Welch, T. W.; Ciftan, S. A.; White, P. S.; Thorp, H. H. *Inorg. Chem.* **1997**, *36* (21), 4812–4821.
- (44) Wasylenko, D. J.; Ganesamoorthy, C.; Henderson, M. A.; Koivisto, B. D.; Osthoff, H. D.; Berlinguette, C. P. *J. Am. Chem. Soc.* **2010**, *132* (45), 16094–16106.
- (45) Arakawa, R.; Kubota, N.; Fukuo, T.; Ishitani, O.; Ando, E. *Inorg. Chem.* **2002**, *41* (14), 3749–3754.
- (46) Miyaji, T.; Kujime, M.; Hikichi, S.; Moro-oka, Y.; Akita, M. *Inorg. Chem.* **2002**, *41* (20), 5286–5295.
- (47) Bennett, M. J.; Donaldson, P. B. *Inorg. Chem.* **1977**, *16* (7), 1585–1589.
- (48) Salles, L.; Piquemal, J.-Y.; Mahha, Y.; Gentil, M.; Herson, P.; Brégeault, J.-M. *Polyhedron* **2007**, *26* (17), 4786–4792.
- (49) Gavrilo, A. L.; Qin, C. J.; Sommer, R. D.; Rheingold, A. L.; Bosnich, B. *J. Am. Chem. Soc.* **2002**, *124* (8), 1714–1722.
- (50) Chishiro, T.; Shimazaki, Y.; Tani, F.; Tachi, Y.; Naruta, Y.; Karasawa, S.; Hayami, S.; Maeda, Y. *Angew. Chem.-Int. Ed.* **2003**, *42* (24), 2788–2791.
- (51) Thewalt, U.; Marsh, R. E. *J. Am. Chem. Soc.* **1967**, *89* (24), 6364–6365.
- (52) Itoh, K.; Hayashi, H.; Furutachi, H.; Matsumoto, T.; Nagatomo, S.; Tosha, T.; Terada, S.; Fujinami, S.; Suzuki, M.; Kitagawa, T. *J. Am. Chem. Soc.* **2005**, *127* (14), 5212–5223.
- (53) Le Carpentier, J. M.; Weiss, R. *Acta Crystallogr.* **1972**, *B28*, 1421–1430.
- (54) Shen, J.; Stevens, E. D.; Nolan, S. P. *Organometallics* **1998**, *17* (18), 3875–3882.
- (55) Khairul, W. M.; Fox, M. A.; Zaitseva, N. N.; Gaudio, M.; Yufit, D. S.; Skelton, B. W.; White, A. H.; Howard, J. A. K.; Bruce, M. I.; Low, P. J. *Dalton Trans.* **2009**, 47, 610–620.
- (56) Bruce, M. I.; Hall, B. C.; Zaitseva, N. N.; Skelton, B. W.; White, A. H. *J. Chem. Soc., Dalton Trans.* **1998**, 11, 1793–1803.
- (57) Kirchner, K.; Mauthner, K.; Mereiter, K.; Schmid, R. *J. Chem. Soc., Chem. Commun.* **1993**, 11, 892–894.
- (58) Morales-Morales, D.; Redon, R.; Cramer, R. E. *Inorg. Chim. Acta* **2001**, *321* (1), 181–184.
- (59) Navarro Clemente, M. E.; Juarez Saavedra, P.; Cervantes Vasquez, M.; Paz-Sandoval, M. A.; Arif, A. M.; Ernst, R. D. *Organometallics* **2002**, *21*, 592–605.